

CO₂ Reduction

International Edition: DOI: 10.1002/anie.201606424

German Edition: DOI: 10.1002/ange.201606424

Tunable Syngas Production from CO₂ and H₂O in an Aqueous Photoelectrochemical Cell

Sheng Chu, Shizhao Fan, Yongjie Wang, David Rossouw, Yichen Wang, Gianluigi A. Botton, and Zetian Mi*

Abstract: Syngas, the mixture of CO and H₂, is a key feedstock to produce methanol and liquid fuels in industry, yet limited success has been made to develop clean syngas production using renewable solar energy. We demonstrated that syngas with a benchmark turnover number of 1330 and a desirable CO/H₂ ratio of 1:2 could be attained from photoelectrochemical CO₂ and H₂O reduction in an aqueous medium by exploiting the synergistic co-catalytic effect between Cu and ZnO. The CO/H₂ ratio in the syngas products was tuned in a large range between 2:1 and 1:4 with a total unity Faradaic efficiency. Moreover, a high Faradaic efficiency of 70% for CO was achieved at underpotential of 180 mV, which is the lowest potential ever reported in an aqueous photoelectrochemical cell. It was found that the combination of Cu and ZnO offered complementary chemical properties that lead to special reaction channels not seen in Cu, or ZnO alone.

Syngas (synthesis gas, CO + H₂ mixtures) is a critical C1 feedstock to produce methanol and synthetic liquid fuels via established industrial process.^[1] For practical applications, the CO/H₂ ratio in syngas mixtures is important to meet the requirements for different downstream products (1:2 and 1:1 for methanol and dimethyl ether, respectively). To date, syngas is predominantly derived from non-renewable fossil sources such as natural gas and coal. CO₂ is a useful carbon source for fuel or chemical synthesis due to its abundance, availability, nontoxicity and recyclability.^[2] Using energy from a renewable source (e.g. solar energy) to reduce CO₂ and H₂O offers an alternate, sustainable and carbon-neutral approach for obtaining syngas mixtures.^[3] Recently, the photoelectrochemical (PEC) route, which mimic natural photosynthesis to directly convert light energy into storable chemical energy at ambient conditions, has attracted substantial interests for

application in CO₂ reduction.^[4] To date, a range of semiconductors, including p-Si,^[5] p-CdTe,^[6] p-InP^[6] and ZnTe,^[7] usually in combination with an effective metal co-catalyst (e.g. Au, Ag and Cu), have been investigated for selective CO formation from CO₂ reduction in an aqueous PEC cell. The device performance, however, often suffers from the following fundamental limitations, including impractically high overpotential (typically >0.5 V) to activate the inert and very stable CO₂ molecule, and low selectivity towards CO due to the similarity in reduction potentials of competitive H₂ evolution reaction and the formation of other CO₂ reduction products (e.g. HCOOH, CH₄). Thus, it is highly desirable to develop high-efficiency materials system with controlled selectivity for CO₂ reduction towards CO at low overpotential or even underpotential without any external electrical bias.

Here, we demonstrate that a monolithically integrated photocathode, by coupling Cu and ZnO as dual co-catalysts with the strong light harvesting of p-n junction Si and efficient electron extraction effect of GaN nanowire arrays (Cu-ZnO/GaN/n⁺-p Si), can efficiently produce syngas from CO₂ and H₂O reduction in an aqueous PEC cell. The CO/H₂ ratio in the syngas product could be adjusted in a large range between 2:1 and 1:4 with a total unity Faradaic efficiency (FE). Moreover, a benchmark turnover number of 1330 and a high FE of 70% for CO at underpotential of 180 mV were achieved. Additionally, the photocathode exhibited superior stability for syngas production under constant illumination for 10 h. Interestingly, it was found that the combination of Cu and ZnO offered synergetic effects that lead to special reaction pathways not seen in Cu or ZnO alone.

The design of Cu-ZnO/GaN/n⁺-p Si photocathode is schematically illustrated in Figure 1a. The sample was synthesized in two steps. First, one-dimensional (1D) GaN nanowire arrays were grown on p-n junction Si wafer by plasma-assisted molecular beam epitaxy. Such a structure takes advantage of the strong light absorption capability of p-n junction Si and efficient electron extraction effect provided by GaN nanowires.^[8] In addition, GaN exhibits a high level of photostability in aqueous solution,^[9] and the nanowire arrays can enhance the light absorption due to the anti-reflection effect.^[10] Second, two-dimensional (2D) ZnO nanosheets and zero-dimensional (0D) Cu nanoparticles were photodeposited on the upper parts of GaN nanowires via a simple wet chemical process (see the Supporting Information (SI) for experimental details). The energy band diagram of the composites under illumination is depicted in Figure S1 (SI). In this multi-dimensional heterostructure, the p-n junction Si can absorb a large number of photons up to wavelengths of 1100 nm due to its narrow band gap ($E_g \approx 1.1$ eV),

[*] Dr. S. Chu, Dr. S. Fan, Dr. Y. Wang, Prof. Z. Mi
Department of Electrical and Computer Engineering
McGill University
3480 University Street, Montreal, QC H3A 0E9 (Canada)

Y. Wang, Prof. Z. Mi
Department of Electrical Engineering and Computer Science, Center
for Photonics and Multiscale Nanomaterials, University of Michigan,
Ann Arbor
1301 Beal Avenue, Ann Arbor, MI 48105 (USA)
E-mail: ztmi@umich.edu

Dr. D. Rossouw, Prof. G. A. Botton
Department of Materials Science and Engineering
McMaster University
1280 Main Street West, Hamilton, Ontario L8S 4L7 (Canada)

Supporting information for this article can be found under:
<http://dx.doi.org/10.1002/anie.201606424>.

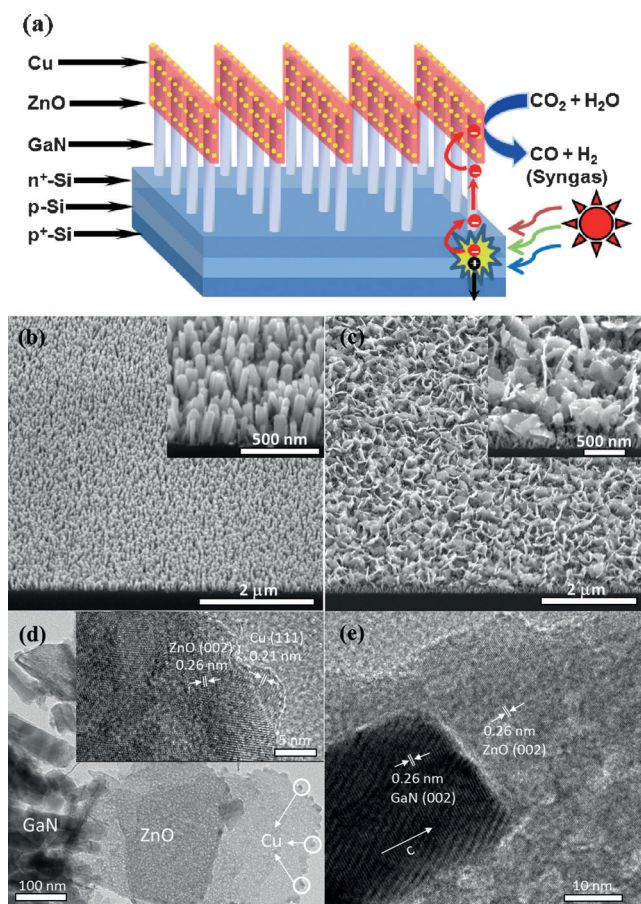


Figure 1. a) Cu-ZnO/GaN/ n^+ -p Si photocathode (not drawn to scale). b) SEM images of GaN nanowires grown on a p-n junction Si. c) SEM and d) TEM images of Cu-ZnO decorated GaN nanowires. Inset of (d), and (e) HRTEM images of the interface between Cu, ZnO and GaN.

while the photogenerated electrons in the Si can be readily injected and transport via the 1D GaN nanowires to 2D ZnO nanosheets due to the small conduction band offsets between them. ZnO could perfectly align with GaN due to their similar crystal structure and very close lattice match.^[11] Therefore, ZnO may form promising junction with GaN to facilitate the transport of photogenerated electrons.^[12] Moreover, ZnO has excellent properties to adsorb and activate inert CO_2 molecule for subsequent reduction steps.^[13] Finally, due to the higher electron affinity of Cu, the energetic electrons can readily reach the Cu nanoparticles for syngas production via the intimate Cu-ZnO interface.

The morphology structure and chemical component of the Cu-ZnO/GaN/ n^+ -p Si heterostructures were studied by scanning electron microscopy (SEM), transmission electron microscopy (TEM) and X-ray photoelectron spectroscopy (XPS). The SEM image of GaN/ n^+ -p Si (Figure 1 b) shows the GaN nanowires are vertically aligned on the Si substrate with lengths and diameters about 150 nm and 30 nm, respectively. After the deposition of Cu-ZnO, it can be seen that the upper part of the GaN nanowires are covered by a network of ZnO nanosheets with sizes in the ranges of 300–500 nm and thicknesses about 10 nm (Figure 1 c). A range of Cu nano-

particles of 3–10 nm size are deposited on the surface of ZnO nanosheets (Figures 1 c,d). The presence of both Cu and Zn in the composites was confirmed by energy-dispersive X-ray (EDX) spectrum (Figure S2). High-resolution (HR) TEM images in Figures 1 d,e show that intimate contacts are formed between GaN nanowires, ZnO nanosheets and Cu nanoparticles, which are beneficial for efficient transport of photogenerated charge carriers.^[14] The lattice fringe of 0.21 nm corresponds to the (111) facet of Cu (inset of Figure 1 d). Both GaN and ZnO show interplanar spacing of 0.26 nm between the two adjacent (002) lattice planes of wurtzite structure, indicating the growth along (0001) direction (c-axis). The (0001) orientation of GaN nanowires is confirmed by the presence of (002) and (004) diffraction peak from X-ray diffraction (XRD) measurement (Figure S3). The XPS analysis indicates metallic Cu (Cu^0) and Zn^{2+} from ZnO (Figure S4).

PEC performance of the Cu-ZnO/GaN/ n^+ -p Si photocathode was evaluated in a conventional three-electrode cell in CO_2 -saturated aqueous solution of 0.5 M KHCO_3 (pH 8) under 300 W xenon lamp irradiation. Figure 2 a shows the FEs

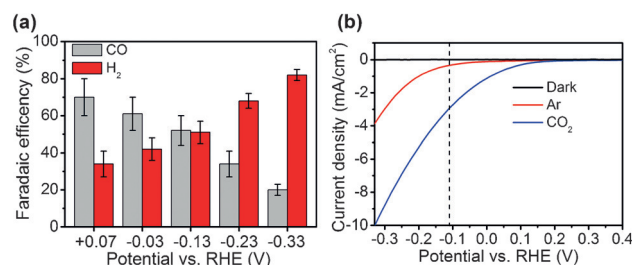


Figure 2. a) FEs for CO (gray bars) and H_2 (red bars) of Cu-ZnO/GaN/ n^+ -p Si photocathode as a function of potential in CO_2 -saturated 0.5 M KHCO_3 solution (pH 8). b) J - V curves in Ar- and CO_2 -saturated 0.5 M KHCO_3 solution. The dashed line shows the standard potential for CO_2 reduction to CO at pH 8.

for CO and H_2 as a function of applied potential between +0.07 V and -0.33 V vs. RHE. The chronoamperometry data and photocurrent-potential curve under chopped illumination are shown in Figures S5 and S6. At an applied potential of +0.07 V, CO is the dominant product with a FE of 70% and the remaining balance of photocurrent drives the reduction of proton to form H_2 . By tuning the potential from +0.07 V to -0.33 V, the CO/ H_2 ratio can be adjusted in a large range between 2:1 and 1:4. At -0.23 V, a CO/ H_2 ratio of 1:2 is obtained, which is a desirable composition of syngas mixtures for methanol and liquid fuels production.^[1] The decreasing of CO selectivity by applying a more negative potential in this study is consistent with previously reported results over Cu-based cathodes.^[15] At low applied bias, CO can be formed at relatively high rate due to the catalytic effect of Cu cathode and lower overpotential required compared to the formation of other CO_2 reduction products (e.g. CH_4). As the overpotential increases, the FE for CO decreases because kinetic mass transfer of CO_2 to the electrode surface instead of thermodynamics becomes the rate-determining step for the CO formation. It was reported that local pH near the cathode

could be substantially higher than that in the bulk electrolyte at high current density operation ($> 1 \text{ mA cm}^{-2}$), owing to the release of OH^- from CO_2 reduction and H_2 evolution. The large increase in pH at the cathode surface would lead to a great reduction in the local CO_2 concentration and thus form a kinetic and mass transport limitation for CO_2 reduction.^[16] The kinetic limitation was evidenced by the fairly constant value of partial current density for CO in the high overpotential region (Figure S7). At all the applied potentials, a total FE of $103 \pm 5\%$ was obtained for the co-generation of CO and H_2 , with no appreciable amount of other gas products detected by GC. Besides, no liquid product (e.g. HCOOH and CH_3OH) was observed in the analysis of electrolyte by nuclear magnetic resonance (NMR) spectroscopy, suggesting a unity FE of our material system for syngas production.

To determine electrode activity with CO_2 , a comparison study of photocurrent-potential curves under Ar and CO_2 atmosphere was conducted (Figure 2b). It was found that there was a strong photocurrent enhancement under the CO_2 atmosphere, which is attributed to the interaction between the electrode surface and CO_2 molecule for producing CO. To verify the evolved CO is derived from CO_2 reduction rather than other possible carbon impurities on the catalyst, we used high-purity $^{13}\text{CO}_2$ as the reactant to conduct the reaction. The $^{13}\text{CO}_2$ isotopic labeling results showed a similar peak at the same retention time in the GC with $^{12}\text{CO}_2$ experiment; however, only a signal at m/z 29 corresponding to ^{13}CO appeared in the mass spectrum data (Figure S8). This provides direct evidence that the CO product is originated from the reduction of CO_2 .

The operating stability of the photoelectrode is essential to their application. Figure 3 shows the chronoamperometry data and FEs for CO and H_2 at -0.23 V vs. RHE under constant illumination for 10 h. The electrode showed no appreciable decay in photocurrent density while maintaining a total near-unity FE for CO and H_2 co-generation. The CO/ H_2 ratio in the products was kept nearly 1:2 during the 10 h period of operation, demonstrating the superior stability of the electrode. The turnover number (TON), defined as the ratio of the total amount of gas evolved ($66.5 \mu\text{mol}$) to Cu-ZnO catalyst ($\approx 0.05 \mu\text{mol}$, see Figure S9 for calculation details), reached 1330 after 10 h of photoelectrolysis, signifi-

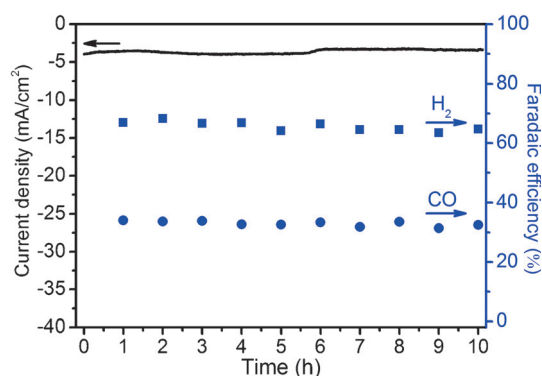


Figure 3. Chronoamperometry data and FEs for CO and H_2 of Cu-ZnO/GaN/ n^+ -p Si photocathode at -0.23 V vs. RHE.

cantly out-performing the values recently reported for selective CO formation from CO_2 reduction.^[17] As a note, the TON reported in this study is underestimated because the calculation is based on the bulk catalyst instead of only surface sites (see the SI for TON calculation considering only surface sites).

An important feature of our system is the high FE of 70% for CO achieved at underpotential of 180 mV ($+0.07 \text{ V}$ vs. RHE), suggesting that light energy is indeed used to drive the reaction. The reported low potentials and FEs for the reduction of CO_2 to CO in an aqueous PEC cell are compared in Table 1. Among various monolithic photocathodes, our

Table 1: The reported low potentials and corresponding FEs for CO in aqueous PEC cell using various monolithic photocathode materials.

Electrode	Co-catalyst	Electrolyte	Potential (V vs. RHE) ^[a]	FE [%]	Ref.
p-Si	–	KHCO_3	–0.62	12	[5]
p-Si	Au	KHCO_3	–0.09	62	[5]
p-Si	Ag	KHCO_3	–0.40	51	[5]
p-Si	Cu	KHCO_3	–0.40	10	[5]
p-CdTe	–	TEAP ^[b]	–0.35	78	[6]
p-InP	–	TEAP	–0.35	31 ^[c]	[6]
p-ZnTe	–	KHCO_3	–0.20	8.4	[7a]
p-ZnTe	Au	KHCO_3	–0.10	26 ^[d]	[7b]
GaN/ n^+ -p Si	Cu/ZnO	KHCO_3	+0.07	70	this work

[a] Reported potentials were converted to RHE values by the following equation: $V_{\text{RHE}} = V + (0.059 \times \text{pH}) + V_{\text{Ref}}$. Where $V_{\text{Ref}} = 0.244$ and 0.197 for SCE and Ag/AgCl, respectively. [b] TEAP: Tetraethylammonium perchlorate. [c] Obtained at -0.55 V vs. RHE, the data at -0.35 V was not reported. [d] The highest FE reported in the system was 63% at -0.5 V vs. RHE.

material exhibits the lowest potential, which is 160 mV positive shifts compared with the lowest potential reported in the literature.^[5] It is worth noting that the onset potential can be further positively shifted by connecting our photocathode with a photovoltaic system. Very recently, Lee and co-workers achieved a very low onset potential of ca. 0.6 V vs. RHE in a photocathode-photovoltaic tandem device.^[7c] Moreover, the CO FE of 70% in this work represents one of the highest values reported in an aqueous PEC cell, which was even more remarkable considering the noble-metal-free component in the present material. The extremely low onset potential of our photocathode is attributed to its multi-functional hierarchical structures, which include the strong light harvesting of p-n junction Si, the efficient electron extraction and transport of GaN nanowire arrays, and the fast surface reaction kinetics of Cu-ZnO co-catalysts. Control experiments of photocurrent-potential test in the absence of one of the three components were conducted (Figure S10). The onset potentials (as taken from the potentials of 0.5 mA cm^{-2}) of the photocathodes without p-n junction Si, GaN nanowires or Cu-ZnO co-catalysts are -0.63 , -0.20 and -0.32 V vs. RHE respectively, which are at least 270 mV more negatively shifted compared to that of Cu-ZnO/GaN/ n^+ -p Si ($+0.07 \text{ V}$).

In order to gain insights into the high performance of Cu-ZnO/GaN/ n^+ -p Si, PEC measurements were conducted with

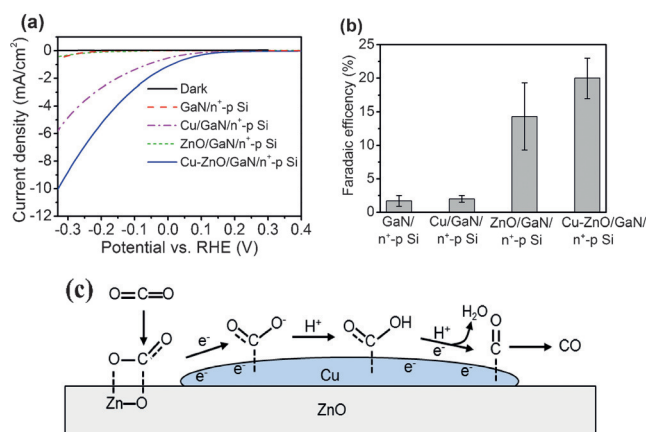


Figure 4. a) *J*-*V* curves. b) FEs for CO at -0.33 V vs. RHE. c) Proposed reaction mechanism for the photoreduction of CO₂ to produce CO on Cu-ZnO dual co-catalysts.

plain GaN/n⁺-p Si and with single Cu or ZnO co-catalyst. Photocurrent-potential curves (Figure 4a) show the photocurrent density is very small in the absence of any co-catalyst (0.6 mA cm^{-2} at -0.33 V vs. RHE), and ZnO alone does not show any promotive effect. In contrast, Cu co-catalyst can greatly enhance the activity, resulting in a photocurrent density of ca. 6 mA cm^{-2} at -0.33 V. Compared to bare Cu, significantly higher photocurrent density of 10 mA cm^{-2} at -0.33 V is attained when Cu and ZnO are loaded simultaneously. A comparison study of FEs for CO of different samples at -0.33 V is shown in Figure 4b. It is clear that Cu has negligible effect on the selectivity for CO₂ reduction to CO, whereas the CO formation selectivity increases about eight times from 1.7% to 14.3% by loading ZnO on GaN/n⁺-p Si. In addition, the FE for CO of Cu-ZnO/GaN/n⁺-p Si is the highest (20%), which is ten times higher than that of Cu/GaN/n⁺-p Si (2%). The important role of ZnO in the selective CO₂ reduction is further confirmed by the comparison of FEs for CO at other potentials range from $+0.07$ V to -0.23 V (Figure S11). Moreover, CO₂ adsorption-desorption testing results (Figure S12) revealed the amount of CO₂ adsorption capacity over Cu-ZnO/GaN/n⁺-p Si was $0.95 \mu\text{mol cm}^{-2}$, which was 3.4 times higher than that of Cu/GaN/n⁺-p Si ($0.28 \mu\text{mol cm}^{-2}$). Note that the CO₂ adsorption amount of plain GaN/n⁺-p Si ($0.24 \mu\text{mol cm}^{-2}$) was only slightly smaller than that of Cu/GaN/n⁺-p Si, indicating the low propensity of Cu co-catalyst for CO₂ adsorption. On the basis of the above results, the reaction mechanism of CO₂ photoreduction to produce CO on Cu-ZnO dual co-catalysts is proposed (Figure 4c). CO₂ molecule is initially adsorbed and activated on ZnO to break its linear symmetry for the formation of destabilized bent configuration. Then it migrates onto Cu to proceed through a series of elementary steps via the carboxyl (*COOH) intermediate involving the consecutive transfer of protons and electrons, resulting in the cleavage of C–O bond and the formation of CO product.^[18] The proposed mechanism was further supported by a systematic study of the effect of Cu/Zn ratio on the product selectivity (Figure S13). It was found that the highest FE for CO was obtained at a composition with a balanced reaction of CO₂ adsorption on ZnO and

proton-coupled electron transfer on Cu. The capability of ZnO to enhance the selectivity for CO₂ reduction to CO was also verified in other similar systems, by coupling ZnO with other metal co-catalysts such as Au and Ag. The FEs for CO with Au-ZnO or Ag-ZnO dual co-catalysts are 1.9 and 2.4 times higher than that with Au or Ag alone, respectively (Figure S14). SEM tests revealed that the sizes of Au or Ag particles were in the range of 50–100 nm and small interface area was formed between the metal and ZnO nanosheets (Figures S15,S16), which may cause less synergetic effect for selective CO₂ reduction to CO.

In addition to the electronic effect to influence the binding of CO₂, there is a geometric effect of ZnO nanosheet to function as an excellent 2D support for the enhanced dispersion of Cu nanoparticles to increase the Cu surface area for the reactions. The SEM image of Cu/GaN/n⁺-p Si shows the sizes of Cu are in the range between 10 and 50 nm, with some particles aggregate to form large clusters up to 100 nm (Figure S17). The possible effect of change in the oxidation states of Cu in the presence of ZnO was ruled out from XPS analysis (Figure S18). However, the Cu2p peak of Cu-ZnO/GaN/n⁺-p Si was negatively shifted by ca. 0.4 eV compared to that of Cu/GaN/n⁺-p Si, which could be attributed to the strong interaction between Cu and ZnO due to the electron transfer from ZnO to Cu.^[19] In the intimate Cu-ZnO interface, one can have adsorption/reaction sites with complementary chemical properties, truly bifunctional sites that cannot be achieved by either Cu or ZnO alone.

In conclusion, we have demonstrated a monolithic photocathode for efficient, stable and tunable syngas production from CO₂ and H₂O reduction in an aqueous PEC cell. An unprecedented TON of 1330 and a high FE of 70% for CO at underpotential of 180 mV were achieved by integrating the strong light absorption capability of p-n junction Si and efficient electron extraction effect of GaN nanowire arrays with the fast surface reaction kinetics of Cu-ZnO co-catalysts. It was found that the combination of Cu and ZnO offered complementary chemical properties that lead to special reaction pathways not seen in Cu or ZnO alone. This work opens up opportunities to develop sustainable and carbon-neutral syngas production from the reduction of CO₂ and H₂O using solar energy with rationally designed heterostructures.

Acknowledgements

This work was supported by the Natural Sciences and Engineering Research Council of Canada (NSERC) and the Climate Change and Emissions Management Corporation (CCEMC). We thank Dr. Lu Li for the GC-MS tests in the ¹³C-labeling experiment.

Keywords: CO₂ reduction · Co-catalysts · energy conversion · semiconductors · solar fuel

How to cite: *Angew. Chem. Int. Ed.* **2016**, *55*, 14262–14266
Angew. Chem. **2016**, *128*, 14474–14478

- [1] A. Indarto, J. Palguandi, *Syngas Production. Application and Environmental Impact*, Nova Science, New York, **2013**.
- [2] G. Centi, S. Perathoner, *Green Carbon Dioxide: Advances in CO₂ Utilization*, Wiley-VCH, Weinheim, **2014**.
- [3] a) V. N. Nguyen, L. Blum, *Chem. Ing. Tech.* **2015**, *87*, 354–375; b) F. Li, J. Lau, S. Licht, *Adv. Sci.* **2015**, *2*, 1500260; c) D. Li, S. Ouyang, H. Xu, D. Lu, M. Zhao, X. Zhang, J. Ye, *Chem. Commun.* **2016**, *52*, 5989–5992.
- [4] a) B. Kumar, M. Llorente, J. Froelich, T. Dang, A. Sathrum, C. P. Kubiak, *Annu. Rev. Phys. Chem.* **2012**, *63*, 541–569; b) J. L. White, M. F. Baruch, J. E. Pander III, Y. Hu, I. C. Fortmeyer, J. E. Park, T. Zhang, K. Liao, J. Gu, Y. Yan, T. W. Shaw, E. Abelev, A. B. Bocarsly, *Chem. Rev.* **2015**, *115*, 12888–12935.
- [5] R. Hinogami, Y. Nakamura, S. Yae, Y. Nakato, *J. Phys. Chem. B* **1998**, *102*, 974–980.
- [6] H. Yoneyama, K. Sugimura, S. Kuwabata, *J. Electroanal. Chem.* **1988**, *249*, 143–153.
- [7] a) J. Jang, S. Cho, G. Magesh, Y. J. Jang, J. Y. Kim, W. Y. Kim, J. K. Seo, S. Kim, K. Lee, J. S. Lee, *Angew. Chem. Int. Ed.* **2014**, *53*, 5852–5857; *Angew. Chem.* **2014**, *126*, 5962–5967; b) Y. J. Jang, J.-W. Jang, J. Lee, J. H. Kim, H. Kumagai, J. Lee, T. Minegishi, J. Kubota, K. Domen, J. S. Lee, *Energy Environ. Sci.* **2015**, *8*, 3597–3604; c) Y. J. Jang, I. Jeong, J. Lee, J. Lee, M. J. Ko, J. S. Lee, *ACS Nano* **2016**, *10*, 6980–6987.
- [8] a) S. Fan, B. Alotaibi, S. Y. Woo, Y. Wang, G. A. Botton, Z. Mi, *Nano Lett.* **2015**, *15*, 2721–2726; b) Y. Wang, S. Fan, B. Alotaibi, Y. Wang, L. Li, Z. Mi, *Chem. Eur. J.* **2016**, *22*, 8809–8813.
- [9] a) M. G. Kibria, R. Qiao, W. Yang, I. Boukahil, X. Kong, F. A. Chowdhury, M. L. Trudeau, W. Ji, H. Guo, F. J. Himpsel, L. Vayssieres, Z. Mi, *Adv. Mater.* **2016**, DOI: 10.1002/adma.201602274; b) M. G. Kibria, Z. Mi, *J. Mater. Chem. A* **2016**, *4*, 2801–2820.
- [10] a) A. M. Mozharov, A. D. Bolshakov, D. A. Kudryashov, N. V. Kryzhanovskaya, G. E. Cirilin, I. S. Mukhin, J. C. Harmand, M. Tchernysheva, *J. Phys. Conf. Ser.* **2015**, *643*, 012115; b) C. Liu, N. P. Dasgupta, P. Yang, *Chem. Mater.* **2014**, *26*, 415–422.
- [11] R. D. Vispute, V. Talyansky, S. Choopun, R. P. Sharma, T. Venkatesan, M. He, X. Tang, J. B. Halpern, M. G. Spencer, Y. X. Li, L. G. Salamanca-Riba, A. A. Iliadis, K. A. Jones, *Appl. Phys. Lett.* **1998**, *73*, 348.
- [12] K. Maeda, T. Takata, M. Hara, N. Saito, Y. Inoue, H. Kobayashi, K. Domen, *J. Am. Chem. Soc.* **2005**, *127*, 8286–8287.
- [13] a) Y. Wang, R. Kovacic, B. Meyer, K. Kotsis, D. Stodt, V. Staemmler, H. Qiu, F. Traeger, D. Langenberg, M. Muhler, C. Woll, *Angew. Chem. Int. Ed.* **2007**, *46*, 5624–5627; *Angew. Chem.* **2007**, *119*, 5722–5725; b) H. Noei, C. Woll, M. Muhler, Y. Wang, *J. Phys. Chem. C* **2011**, *115*, 908–914; c) B. Mei, A. Becerikli, A. Pougin, D. Heeskens, I. Sinev, W. Grunert, M. Muhler, J. Strunk, *J. Phys. Chem. C* **2012**, *116*, 14318–14327.
- [14] E. S. Kim, N. Nishimura, G. Magesh, J. Y. Kim, J. W. Jang, H. Jun, J. Kubota, K. Domen, J. S. Lee, *J. Am. Chem. Soc.* **2013**, *135*, 5375–5383.
- [15] a) D. Raciti, K. J. Livi, C. Wang, *Nano Lett.* **2015**, *15*, 6829–6835; b) C. W. Li, M. W. Kanan, *J. Am. Chem. Soc.* **2012**, *134*, 7231–7234; c) K. P. Kuhl, T. Hatsukade, E. R. Cave, D. N. Abram, J. Kibsgaard, T. F. Jaramillo, *J. Am. Chem. Soc.* **2014**, *136*, 14107–14113.
- [16] a) M. R. Singh, E. L. Clark, A. T. Bell, *Phys. Chem. Chem. Phys.* **2015**, *17*, 18924–18936; b) N. Gupta, M. Gattrell, B. MacDougall, *J. Appl. Electrochem.* **2006**, *36*, 161–172.
- [17] a) H. Takeda, K. Ohashi, A. Sekine, O. Ishitani, *J. Am. Chem. Soc.* **2016**, *138*, 4354–4357; b) T. E. Rosser, C. D. Windle, E. Reisner, *Angew. Chem. Int. Ed.* **2016**, *55*, 7388–7392; *Angew. Chem.* **2016**, *128*, 7514–7518.
- [18] a) A. A. Peterson, F. Abild-Pedersen, F. Studt, J. Rossmeisl, J. K. Nørskov, *Energy Environ. Sci.* **2010**, *3*, 1311–1315; b) S. Back, M. S. Yeom, Y. Jung, *ACS Catal.* **2015**, *5*, 5089–5096.
- [19] F. Liao, Y. Huang, J. Ge, W. Zheng, K. Tedsree, P. Collier, X. Hong, S. C. Tsang, *Angew. Chem. Int. Ed.* **2011**, *50*, 2162–2165; *Angew. Chem.* **2011**, *123*, 2210–2213.

Received: July 10, 2016

Revised: September 28, 2016

Published online: October 14, 2016